



Ultra-fine Cu clusters decorated hydrangea-like titanium dioxide for photocatalytic hydrogen production

Ya-Jie Feng, Yang Wang, Kai-Wen Wang, Jiang-Ping Ma, You-Yu Duan, Jie Liu, Xu Lu, Bin Zhang* , Guo-Yu Wang, Xiao-Yuan Zhou* 

Received: 4 March 2021 / Revised: 30 April 2021 / Accepted: 26 May 2021 / Published online: 8 September 2021
© Youke Publishing Co., Ltd. 2021

Abstract Hydrogen, with the merits of zero emissions and high energy density, is one of the promising green energy sources. Seeking for high efficiency and low-cost catalysts is one of the key issues for hydrogen evolution and its practical applications. Nano-structured metal co-catalysts are widely used to improve the photocatalytic performance via surface electronic structure/properties optimization of the catalyst. Herein, we report ultra-fine (~ 1 nm) Cu clusters decorated hydrangea-like TiO_2 systems for photocatalytic hydrogen evolution. The pristine hydrangea-like TiO_2 support shows a promising performance of hydrogen evolution ($1.8 \text{ mmol}\cdot\text{h}^{-1}\cdot\text{g}^{-1}$), which is ~ 10.7 times higher than that of the commercial P25 ($168 \mu\text{mol}\cdot\text{h}^{-1}\cdot\text{g}^{-1}$). After ultra-fine Cu clusters

decoration, a maximal hydrogen evolution performance ($3.7 \text{ mmol}\cdot\text{h}^{-1}\cdot\text{g}^{-1}$) is achieved in the optimized system $6\text{Cu}\text{-TiO}_2$ (6 wt%). Experimental and theoretical studies demonstrate that the ultra-fine Cu clusters decoration could promote the charge separation and transfer process effectively. The Cu clusters also act as reaction sites for reduction of H_2O to H_2 . These results are of great importance for the study of Cu-based co-catalyst systems and also shed light on the development of other non-noble metal co-catalysts in photocatalysis hydrogen evolution.

Keywords Photocatalysis; Hydrangea-like TiO_2 ; Ultra-fine Cu clusters; Hydrogen evolution; Charge separation and transfer

Supplementary Information The online version contains supplementary material available at <https://doi.org/10.1007/s12598-021-01815-z>.

Y.-J. Feng, Y. Wang, J.-P. Ma, Y.-Y. Duan,
X. Lu, X.-Y. Zhou*
College of Physics and State Key Laboratory of Coal Mine
Disaster Dynamics and Control, Chongqing University,
Chongqing 401331, China
e-mail: xiaoyuan2013@cqu.edu.cn

Y.-J. Feng, G.-Y. Wang
Chongqing Institute of Green and Intelligent Technology,
Chinese Academy of Sciences, Chongqing 400722, China

K.-W. Wang
Institute of Microstructure and Properties of Advanced
Materials, Beijing University of Technology, Beijing 100124,
China

J. Liu, B. Zhang*
Analytical and Testing Center, Chongqing University,
Chongqing 401331, China
e-mail: welon5337@126.com

1 Introduction

The energy crisis and environmental pollution caused by the use of non-renewable energy sources, such as coal, oil and other fossil fuels, have become two major issues, which restrict the sustainable development of human beings. It is highly desirable to seek for green and reproduction energy sources [1, 2]. Hydrogen, with the merits of zero emissions and high energy density values per unit mass, is one of the promising candidates for green energy sources [3]. The current hydrogen production technology mainly includes methanol steam reforming reaction, hydrogen production from natural gas, electrocatalysts for water splitting, etc. [4]. Among various hydrogen production technologies, photocatalytic water splitting is considered to be one of the most promising and environmental-friendly techniques [5, 6]. Since the discovery of photoelectrochemical (PEC) water splitting in 1972 [7], TiO_2 has attracted intensive attention as photocatalytic materials for



its appropriate energy band position, high chemical stability, low cost and non-toxicity [8–16]. However, the intrinsic shortcomings of TiO_2 , e.g., slow electron transfer and rapid recombination of photogenerated charge carriers drastically, have limited their practical applications [17].

To improve the photocatalytic activity, co-catalysts are usually introduced/decorated onto the surface of semiconductors/supports (e.g., TiO_2) [3, 18–20]. Nowadays, the noble metal Pt is reported as a state-of-the-art co-catalyst for the photocatalytic hydrogen evolution [21–23]. However, the application of Pt-based co-catalysts is still restricted by its high cost and scarcity. Size reduction of co-catalyst to nano-scale and even single atoms was widely applied to improve utilization efficiency of noble elements for cost reduction and catalytic performance promoting simultaneously [24–27]. For example, in 2014, Xing et al. [28] reported that 6–13-fold enhancement of the photocatalytic hydrogen evolution was achieved when the Pt clusters were down to single atoms on the TiO_2 support. Meanwhile, non-noble metal (e.g., Fe, Co, Ni, Cu) co-catalysts are another way to reduce cost and facilitate the practical applications [29–32]. For instance, as Ni atoms were introduced on the supports (e.g., TiO_2 [33] or C_3N_4 [34]), the photocatalytic performance of the systems has been improved significantly. Aside from the co-catalysts, designing/optimizing the support materials is also employed as an alternative route to promote the catalytic performance. For support materials, surface area increasing through specific nano-morphology and electronic structure modulation via doping or defects engineering seems to be efficient approaches [17, 18, 35–38]. For example, the hierarchical TiO_2 with large specific surface areas of $170 \text{ m}^2\cdot\text{g}^{-1}$ shows excellent photocatalytic performance than the commercial P25 ($\sim 45 \text{ m}^2\cdot\text{g}^{-1}$) [39]. This is because the enlarged surface area would result in more exposure active sites and solid interfaces which play vital roles on the photocatalytic reactions.

To promote the photocatalytic reaction, the photogenerated electrons and holes must be separated and transferred from the bulk phase to the active sites to drive redox reactions [40–42]. Actually, photocatalytic activity is generally charge separation and transfer dependence [43]. Metal clusters (especially ultra-fine clusters or fully exposed cluster catalysts (FECC) [44]) are found to have better performance in tuning the surface electronic properties and subsequently accelerate the charge separation and transfer process [45–48]. Wang et al. [45] reported that the photocatalytic reaction was boosted by Pd (containing both single atoms and clusters) loaded onto TiO_2 . It was suggested that the Pd clusters promote the photogenerated charge separation and provide the optimum active sites for H_2 evolution. Interestingly, Yan et al. [47] found that the charge was transferred from Pt single atoms to the sulfur-

doped carbon supports, but contrarily, for the ultra-small Pt clusters ($\sim 1.5 \text{ nm}$), the transfer direction was reversed, i.e., from the support to Pt clusters. In the last few years, Cu species co-catalysts (both nanoparticles and single atoms) have drawn wide attention due to their competitive performance, low-cost and natural abundance [3, 43]. In 2019, Lee et al. [49] designed and synthesized highly active TiO_2 decorated with Cu single atoms for photocatalytic hydrogen evolution. Seadira et al. [50] found that Cu-doped TiO_2 material prepared by impregnation method had better hydrogen evolution activity than Co, Cr, Ag and Ni, respectively. However, there are fewer reports concerned about the ultra-fine Cu clusters co-catalysts for photocatalytic hydrogen evolution.

In this study, a hydrangea-like TiO_2 support with enhanced photocatalytic performance is synthesized via a simple hydrothermal method. An improved hydrogen evolution rate ($1.8 \text{ mmol}\cdot\text{h}^{-1}\cdot\text{g}^{-1}$) of this hydrangea-like TiO_2 is achieved, ~ 10.7 times higher than that of P25 ($168 \mu\text{mol}\cdot\text{h}^{-1}\cdot\text{g}^{-1}$). Then, ultra-fine ($\sim 1 \text{ nm}$) Cu clusters were further loaded onto the hydrangea-like TiO_2 supports (denoted as Cu- TiO_2). A maximal hydrogen evolution value of $3.7 \text{ mmol}\cdot\text{h}^{-1}\cdot\text{g}^{-1}$ is obtained in the optimized system of 6Cu- TiO_2 (6 wt% Cu), which is about twofold enhancement on the base of the bare hydrangea-like TiO_2 . The experimental and theoretical analysis stress that the enhanced hydrogen production should be attributed to the promoted charge separation and transfer, which originate from the surface electronic properties tuned by the ultra-fine Cu clusters. These results not only fill the gaps of Cu ultra-fine clusters in the study of Cu-based co-catalysts, but also provide guidance for the development of non-noble metal co-catalysts.

2 Experimental

2.1 Materials and chemicals

Titanium butoxide ($\text{Ti}(\text{OBu})_4$), acetic acid (CH_3COOH) and cupric acetate monohydrate ($\text{Cu}(\text{CH}_3\text{COO})_2\cdot\text{H}_2\text{O}$) purchased from Shanghai Aladdin Bio-Chem Technology Co., Ltd., were of analytical grade.

2.2 Materials synthesis of hydrangea-like TiO_2 and XCu- TiO_2 (where X is mass percent of Cu)

The synthesis procedure of the hydrangea-like Cu- TiO_2 is as following. 30 ml CH_3COOH and a certain amount $\text{Cu}(\text{CH}_3\text{COO})_2\cdot\text{H}_2\text{O}$ (0.0176 g, 0.0352 g, 0.0528 g, 0.0704 g) were added into a 50 ml Teflon-lined stainless steel autoclave with stirring. Subsequently, 1 ml $\text{Ti}(\text{OBu})_4$ was added drop-wise to acetic acid solution followed with

5-min stirring. Then, the autoclave was kept at 140 °C for 24 h. The obtained powder samples were washed several times with water and alcohol and dried at 60 °C overnight. The samples were further annealed at 450 °C for 3 h. Finally, the hydrangea-like TiO₂ with Cu decoration were obtained and denoted as 3Cu–TiO₂, 6Cu–TiO₂, 9Cu–TiO₂, 12Cu–TiO₂, respectively. The pure hydrangea-like TiO₂ was prepared under the same condition without the presence of Cu(CH₃COO)₂·H₂O.

2.3 Material characterization

X-ray diffraction (XRD) patterns were carried out using a PANalytical X'Pert apparatus (Netherlands) operated at Cu K α radiation to study the crystal structures of the samples. Raman spectroscopy was collected on a LabRAMM HR evolution imaging microscope system. Transmission electron microscopy (TEM, Thermoscientific Talos F200S) and scanning electron microscopy (SEM, Thermoscientific Quattro S) equipped with energy-dispersive X-ray spectroscopy (EDS) were utilized to investigate the microstructure (crystal structure, morphology, chemical composition) of the samples. The high-angle annular dark-field scanning transmission electron microscopy (HAADF-STEM) image was collected on a probe-corrected FEI Titan Themis microscope at 300 kV. The Brunner–Emmet–Teller (BET) surface areas were analyzed by N₂ adsorption on Unicube (Elementar). X-ray photoelectron spectroscopy (XPS, Thermoscientific ESCALAB250Xi, Al K α) was performed to explore the surface chemical states, where the C 1s peak at 284.8 eV (i.e., the surface adventitious carbon) was used for calibration. Ultraviolet–visible (UV–Vis) spectra were collected on Shimadzu UV-3600 spectrometer (BaSO₄ as a reference background, absorbance was calculated by the Kubelka–Munk method). Time-resolved fluorescence emission spectra (TRPL) were collected on a fluorescence spectrophotometer (FLS1000). A steady-state fluorescence spectrometer (Shimadzu RF-6000) was utilized to measure the photoluminescence (PL) spectra.

2.4 Photocatalytic hydrogen evolution

Photocatalytic hydrogen evolution reactions were performed on a Pyrex vessel connected to a glassed closed circulation and evacuation system (Beijing Perfect Light Company). A 300 W Xe lamp was used as the light source. As for the reaction, 20 mg photocatalysts were dispersed into 100 ml 10 vol% aqueous solution methanol. First, the slurry in the reactor was vacuumed for 30 min to eliminate the dissolved gas molecular and provide an anaerobic condition for the reaction. During the photocatalytic

performance tests, the catalyst was kept in suspension by continuous magnetic stirring at 25 °C (controlled by cooling circulating water). The evolved H₂ was measured by chromatograph (GC7900, Techcomp) with a thermal conductivity detector (TCD) using Ar as the carrier gas.

2.5 Photoelectrochemical measurements

The electrochemical impedance spectroscopy (EIS), Mott–Schottky (MS) and photocurrent were measured by electrochemical workstation (Zahner CIMPS-2). All the measurements were performed on a standard three-electrode system using Pt plate as the counter electrode, Ag/AgCl electrode as reference electrode and 0.5 ml Na₂SO₄ as the electrolyte. The working electrode (glassy carbon electrode) was made as follows: 5 mg above photocatalyst was dispersed into the mixture of 50 μ l Nafion and 950 μ l ethanol with ultrasonication for about 30 min to form a uniform dispersion of the catalysts. Then, 10 μ l of the solution was deposited on the glassy carbon electrode and subsequently dried in air at room temperature.

2.6 Density functional theory calculations

The calculations were carried out based on density functional theory (DFT) utilizing the Vienna ab initio Simulation Package (VASP) [51, 52] with spin-polarized Perdew–Burke–Ernzerh generalized gradient approximation (GGA-PBE) function [53, 54]. The kinetic cutoff energy was set as 500 eV for all calculations, 25% larger than the recommended largest value of component species, sufficiently ensuring calculation accuracy. The DFT-D3 method was used to describe the van der Waals interactions between the adsorbed species and the catalyst [55]. The slab model of anatase surface containing 3 TiO₂ layers and 216 atoms was constructed along *z*-direction. The thick vacuum space was set to 2 nm to avoid interactions between the adjacent models. Moreover, the bottom two atomic layers were fixed, while the uppermost layers and adsorbed cluster molecules were relaxed during all calculations. An Γ -centered 1 \times 2 \times 1 grid was used, and the energy convergence was chosen as 1 \times 10^{−4} eV. The slab model was fully relaxed until the residual forces of each atom less than 0.2 eV·nm^{−1}. To investigate the effect of ultra-fine Cu clusters on the hydrangea-like TiO₂, difference charge density analysis was performed. The difference in charge density is defined as $\Delta\rho = \rho(\text{system}) - \rho(\text{substrate}) - \rho(\text{Cu}_{13})$, where (system) denotes the charge density of the whole system, (substrate) denotes the charge density of TiO₂, and (Cu₁₃) denotes the charge density of Cu₁₃ removing substrate.

3 Results and discussion

3.1 Structure characterization and chemical composition analysis

SEM images (Fig. 1a, d) show that the obtained samples have hydrangea-like sphere structure, with diameter of $\sim 5 \mu\text{m}$. Each sphere is made up of ultra-thin 2D nanosheets radiating out from its center. The hydrangea-like structure of Cu–TiO₂ can be almost maintained after Cu decoration, as the morphology of 6Cu–TiO₂ shows in Fig. 1b, e. SEM–EDS mapping analysis shows that the Cu clusters are uniformly dispersed over TiO₂ (Fig. 1c), which is further confirmed by HAADF observation (Fig. 1h). TEM was further conducted to uncover the microstructure of pure TiO₂ and 6Cu–TiO₂. High-resolution transmission electron microscopy (HRTEM) images (Fig. 1f, g) reveal that the TiO₂ nanosheets in the hydrangea sphere have a typical size of several tens of nanometers with good crystallinity. The measured *d*-spacing of lattice fringe (0.35 nm) could be ascribed to the (101) planes of anatase TiO₂. Furthermore, HAADF–STEM image (Fig. 1h) shows the

uniformly dispersed ultra-fine Cu clusters with average size of $\sim 1 \text{ nm}$. Additionally, these Cu clusters exhibit non-crystalline structure with no regular fringes observed.

As shown in Fig. 2a, all XRD patterns of the samples can be well indexed to anatase TiO₂ phase (JCPDS card No. 21–1272) without detection of any impurities. No diffraction peaks of Cu crystals are observed due to (1) the low loading amount and (2) the non-crystalline structure of the ultra-fine Cu clusters (as confirmed by the above HAADF analysis). The anatase structure is further confirmed by Raman spectroscopy, as shown in Fig. 2b. The major Raman peaks appeared at 143.0, 196.6, 395.9, 515.9 and 639.6 cm^{-1} can be definitely assigned to E_g(1), E_g(2), B_{1g}(1), A_{1g} + B_{1g}(2) and E_g(3) of anatase TiO₂, respectively [29, 56, 57]. BET adsorption–desorption isotherms and pore size distribution of P25, the hydrangea-like TiO₂ and 6Cu–TiO₂ samples were further studied, as shown in Fig. 2c, d. Type IV isotherms are observed for the pure hydrangea-like TiO₂ and 6Cu–TiO₂ catalysts, indicating that there is mesoporous in both samples. The detailed values of the BET surface area, pore volume and average pore diameter of P25 and the hydrangea-like samples are

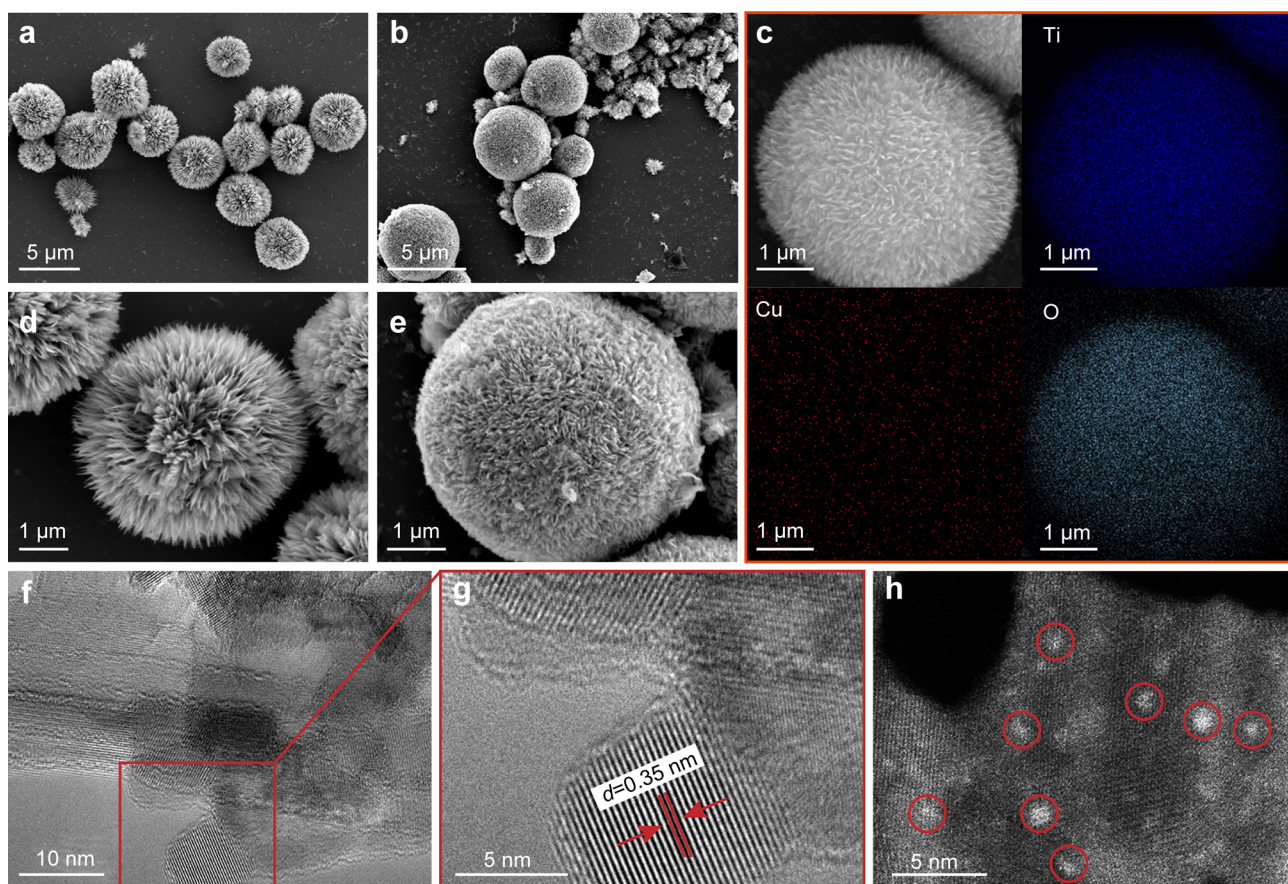


Fig. 1 a, d SEM images of pure TiO₂; b, e SEM images of 6Cu–TiO₂ samples; c SEM–EDS mapping of 6Cu–TiO₂; f, g TEM images of pure TiO₂; h STEM–HAADF image of 6Cu–TiO₂ (several Cu clusters are marked by red circles)

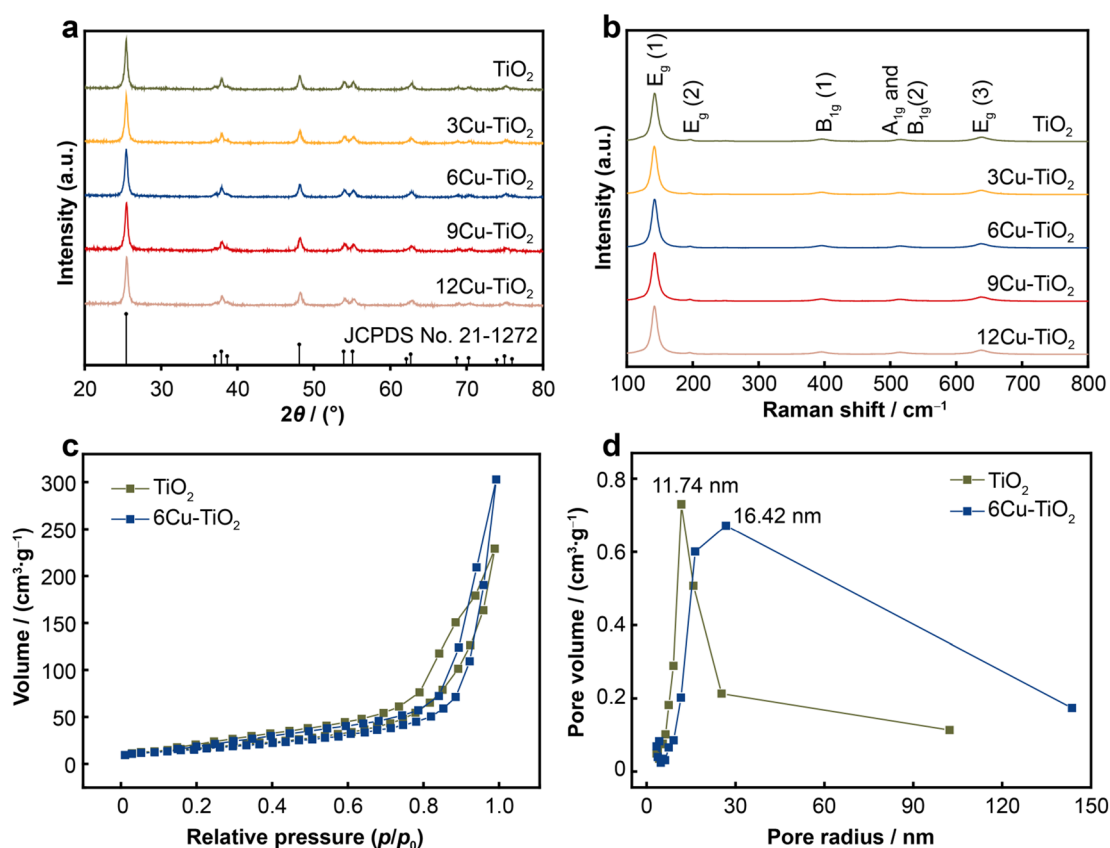


Fig. 2 a XRD patterns and b Raman spectra of samples; c N₂ adsorption/desorption isotherm and d corresponding pore size distribution curves of TiO₂ and 6Cu-TiO₂

presented in Table 1. Similar BET surface areas between the hydrangea-like TiO₂ and 6Cu-TiO₂ (both larger than that of P25) indicate the almost unchanged morphology and surface structure of the hydrangea-like TiO₂ after Cu decoration. However, the pore volume and average pore diameter of the 6Cu-TiO₂ are slightly increased compared with the pristine hydrangea-like TiO₂.

XPS technique was conducted to investigate surface chemical states of the samples. Figure 3a presents the high-resolution XPS spectrum of Ti 2p. The peaks located at 458.75 and 464.48 eV, suggesting that the chemical state of Ti is in the form of Ti⁴⁺ [43], i.e., TiO₂. Figure 3b shows the O 1s spectrum, consisting of a doublet at binding energies of 529.95 and 531.73 eV, which can be deemed as the lattice oxygen (Ti-O-Ti) and Ti-OH, respectively [58].

Basically, 6Cu-TiO₂ exhibits similar characteristic peaks to the pure TiO₂ in the Ti 2p and O 1s. In addition, the Cu peaks can be also observed in 6Cu-TiO₂, as shown in Fig. 3c. The two peaks, i.e., Cu 2p_{3/2} at 933.29 eV and Cu 2p_{1/2} at 953.40 eV, can correspondingly be assigned to the mixture of Cu⁺ and Cu⁰ due to the similar (almost indistinguishable) binding energies between these two species [43].

4 Charge separation and transportation

The separation efficiency and migration of photogenerated charge carriers are closely related to the photocatalytic activity. To understand the effect of the ultra-fine Cu

Table 1 Specific surface areas, average pore sizes and pore volumes of P25, pure TiO₂ and 6Cu-TiO₂ samples

Sample	$S_{\text{BET}}/(\text{m}^2\cdot\text{g}^{-1})$	Pore volume/ $(\text{cm}^3\cdot\text{g}^{-1})$	Average pore diameter/nm
P25	54.164	0.332	3.379
TiO ₂	63.045	0.356	11.742
6Cu-TiO ₂	60.843	0.466	16.419

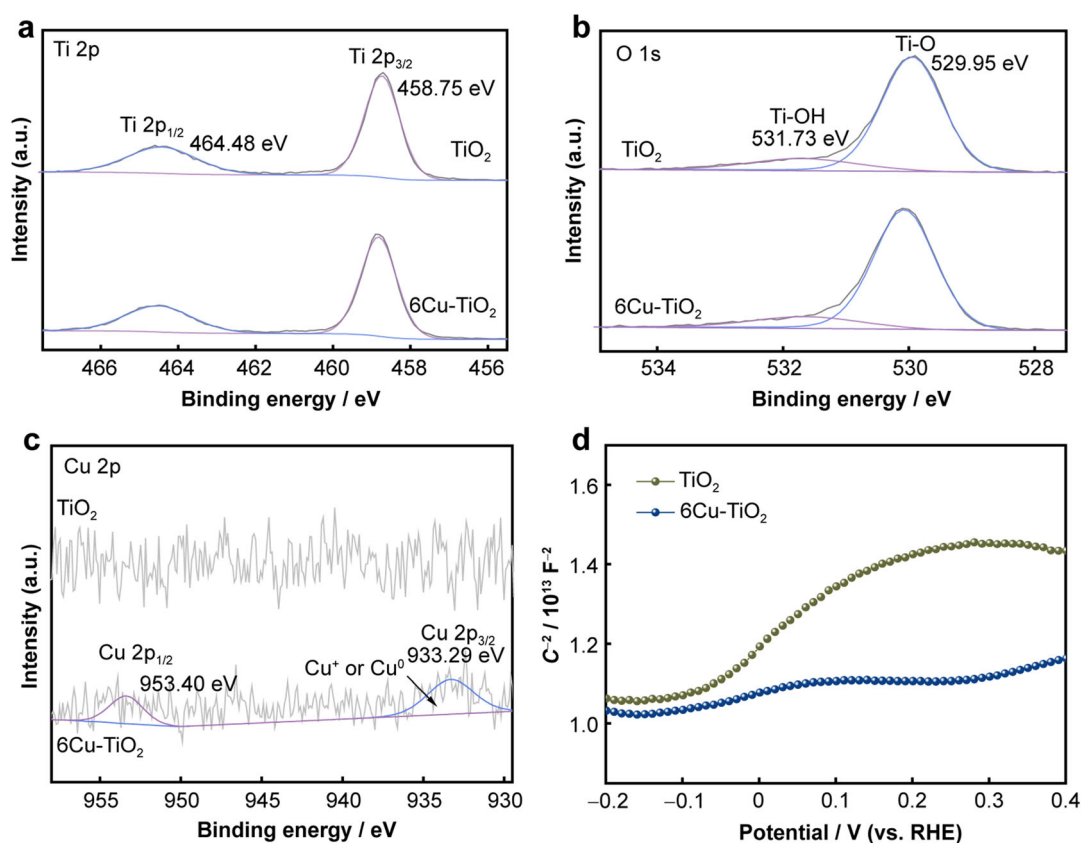


Fig. 3 XPS spectra of TiO_2 and 6Cu-TiO_2 : **a** Ti 2p, **b** O 1s and **c** Cu 2p; **d** Mott–Schottky plots of TiO_2 and 6Cu-TiO_2

clusters on the TiO_2 , the carrier concentration (N_d) was evaluated by the MS test (Fig. 3d), which can be calculated from the slope of MS curves according to the following Eq. (1) [33, 43, 59]:

$$N_d = \frac{2}{e_0 \varepsilon_0 \varepsilon_r} (dC^{-2}/dV)^{-1} \quad (1)$$

where e_0 is the elemental charge (1.60×10^{-19} C), ε_0 is the permittivity of vacuum (8.85×10^{-12} F·m $^{-1}$), and ε_r is the dielectric constant (48.0). It is assumed that the e_0 , ε_0 and ε_r are the same for both TiO_2 and 6Cu-TiO_2 . The obtained N_d value of the 6Cu-TiO_2 (6.40×10^{15}) is nearly 3.4 times larger than that of the pure hydrangea-like TiO_2 (1.90×10^{15}). The higher N_d in the 6Cu-TiO_2 means better electric conductivity and faster charge transfer, which promotes the hydrogen evolution.

The PL and TRPL spectral analyses were carried out for understanding the influence of ultra-fine Cu clusters decorated on the TiO_2 . Figure 4a shows PL emission spectra, in which the intensity of Cu-TiO_2 catalysts decreases compared to the pure TiO_2 , and the smallest one is found in the 6Cu-TiO_2 system. Generally, the lower PL intensity suggests lower recombination rate of photogenerated charge carriers. Thus, it is deduced that the decoration of Cu clusters helps restrain the recombination of

photogenerated charge carriers. In addition, the TRPL spectra were measured to probe the photophysical properties of TiO_2 and 6Cu-TiO_2 (Fig. 4b). Biexponential fittings were applied to analyze the luminescence decay curves (inset in Fig. 4b). The decay kinetics of 6Cu-TiO_2 exhibits a short average lifetime (1.89 ns) as compared to the pure TiO_2 (2.26 ns), which implies the existence of effective electron transfer channels between the TiO_2 support and Cu clusters. Furthermore, the electron transfer rate (k_{ET}) and efficiency (η_{ET}) can be obtained by Eqs. (2, 3) [60]:

$$k_{\text{ET}} = \frac{1}{\tau_{\text{ave}(6\text{Cu-TiO}_2)}} - \frac{1}{\tau_{\text{ave}(\text{TiO}_2)}} \quad (2)$$

$$\eta_{\text{ET}} = 1 - \frac{\tau_{\text{ave}(6\text{Cu-TiO}_2)}}{\tau_{\text{ave}(\text{TiO}_2)}} \quad (3)$$

The k_{ET} and η_{ET} of 6Cu-TiO_2 are 8.67×10^7 s $^{-1}$ and 16.37%, respectively, compared to that of the pure TiO_2 , indicating that ultra-fine Cu clusters can promote the charge transfer between TiO_2 support and Cu clusters effectively. 6Cu-TiO_2 shows larger photocurrent intensity (about 8 times) than the pure TiO_2 (Fig. 4c), confirming that the TiO_2 has better charge generation and migration capabilities after ultra-fine Cu clusters decoration which is further proved by EIS (Fig. 4d). The semicircle in the

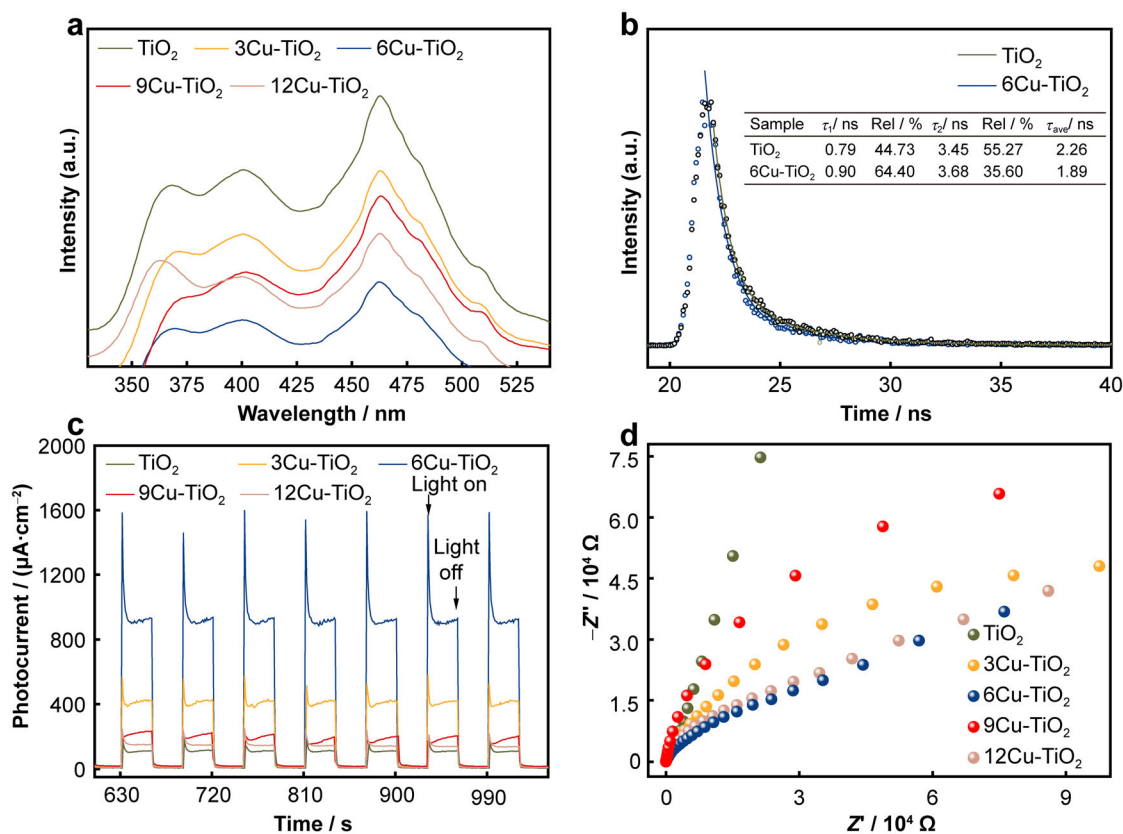


Fig. 4 **a** PL spectra of samples; **b** TRPL decay curves for TiO₂ and 6Cu-TiO₂ and (inset) parameters of time-resolved photoluminescence decay curve determined by biexponential fitting, where τ_1 and τ_2 are values of the lifetime of each decay component and Rel represent the normalized amplitudes (or weighing factors); **c** photocurrent responses of samples, **d** Nyquist plot of EIS (Z' : real part of impedance; $-Z''$: imaginary part of impedance)

Nyquist plot at high frequency represents the charge transfer process, in which the smaller arc of the semicircle means smaller charge resistance and higher electron mobility. As shown in Fig. 4d, the Nyquist plot of 6Cu-TiO₂ at high frequency shows a smaller arc of the semicircle than that of TiO₂, which implies a much lower charge transfer resistance of 6Cu-TiO₂. The above results demonstrate that the charge carrier transfer and separation are promoted by the introduction of ultra-fine Cu clusters onto TiO₂.

4.1 Photocatalytic H₂ evolution activity

In this work, the pure hydrangea-like TiO₂ shows excellent performance (1.8 mmol·h⁻¹·g⁻¹) for hydrogen production which is ~ 10.7 times that of P25 (168 µmol·h⁻¹·g⁻¹), as illustrated in Fig. 5a. Moreover, to explore the relationship between the amount of ultra-fine Cu clusters and the photocatalytic activity in the Cu-TiO₂ systems, photocatalytic reduction of H₂ evolution reactions was conducted. Generally, the photocatalytic

activity was promoted in the Cu-TiO₂ systems (Fig. 5a), suggesting that the introduction of ultra-fine Cu clusters is beneficial for the photocatalytic H₂ evolution. Initially, the H₂ evolution rate increases from 1.8 mmol·g⁻¹·h⁻¹ (TiO₂) to 3.7 mmol·g⁻¹·h⁻¹ (6Cu-TiO₂), about twofold enhancement with the loading amount of ultra-fine Cu clusters increasing from 0 wt% to 6 wt%. In contrast, with the further increase in Cu loading amount to 12 wt% (12Cu-TiO₂), the activity of the catalyst begins to slightly decline, which might be attributed to the decrease in active sites. Furthermore, the activity of photocatalyst is merely decreased slightly after four cycles (Fig. 5b). XRD pattern (Fig. S1) and SEM image (Fig. S2) of the catalyst (6Cu-TiO₂) after cycles of photocatalytic hydrogen evolution activity test were collected. No obvious changes neither in structure nor morphology were found, suggesting good stability of the Cu-TiO₂ systems. While the slight decrease in the photocatalyst performance may be attributed to the interaction disruption between the ultra-fine Cu cluster and the surface of TiO₂.

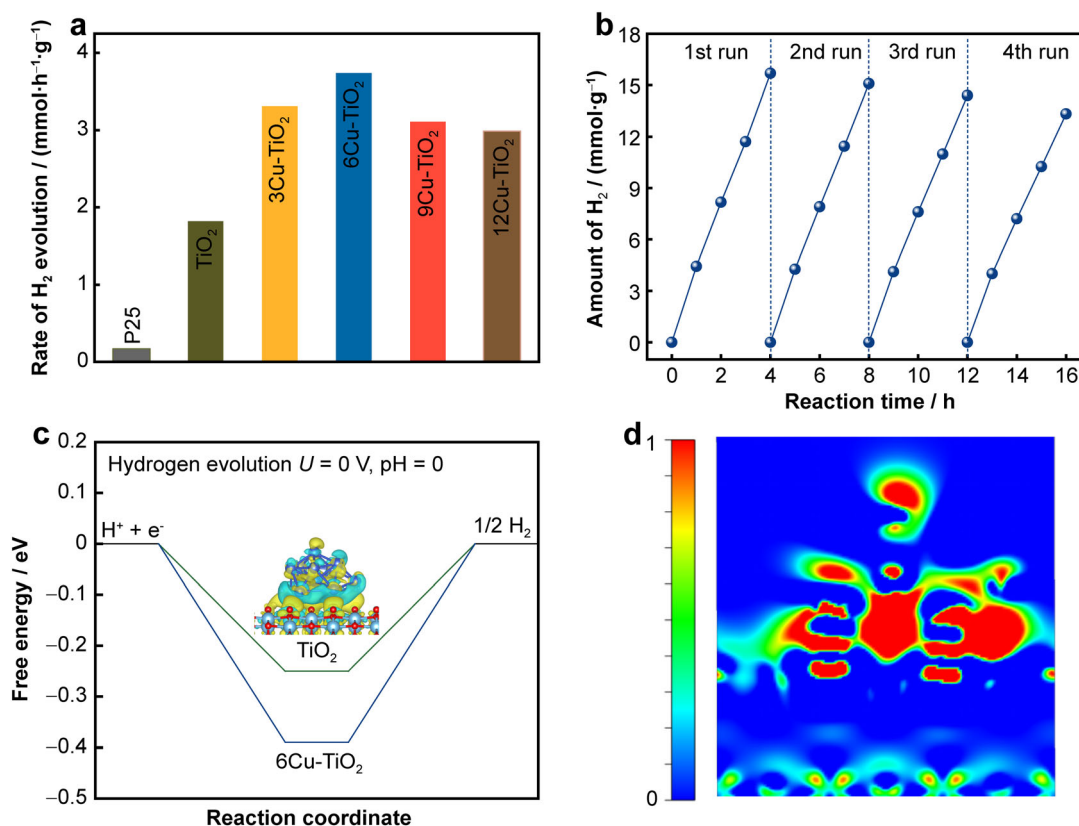


Fig. 5 **a** H₂ evolution rate of samples; **b** cycle stability of 6Cu-TiO₂; **c** free energy versus reaction coordinates of TiO₂ and 6Cu-TiO₂ and (inset) 3D differential charge density of 6Cu-TiO₂; **d** 2D differential charge density of 6Cu-TiO₂, where yellow and blue colors represent positive and negative, respectively

4.2 Photocatalytic mechanism

DFT calculations were performed for analyzing Gibbs free energy (Fig. 5c), the difference of charge density between TiO₂ and 6Cu-TiO₂ (Fig. 5d) and band structures (Fig. S3). Firstly, a higher charge density at the Cu cluster, particularly near the interface of Cu cluster and TiO₂ support, is found in Cu-TiO₂ systems, suggesting that the electrons tend to transfer from TiO₂ to Cu cluster. Therefore, the enhanced charge transfer efficiency could be expected, which is consistent with the above results of higher N_d in 6Cu-TiO₂ than in pure TiO₂. Secondly, with the decoration of ultra-fine Cu clusters, newly generated bands appear in the vicinity of the Fermi level, as seen in the band structure of TiO₂ and 6Cu-TiO₂ in Fig. S3. Finally, as shown in Fig. 5c, the hydrogen adsorption (ΔG) of 6Cu-TiO₂ is -0.16 eV, manifesting much more favorable H₂ evolution activity than the pure TiO₂ (-0.25 eV). The existence of Cu ultra-fine cluster may contribute to the optimal ΔG by tuning the electronic structures of 6Cu-TiO₂. These theoretical results further suggest that the

improved charge separation and transfer can be achieved after loading Cu clusters, which gives rise to the excellent photocatalytic hydrogen production.

UV-Vis absorption spectra in Fig. 6a reveal that after Cu clusters loading onto the surface of TiO₂, absorbance in the range of 400–800 nm is observed, which means enhancement of the visible light absorption. The bandgap of 6Cu-TiO₂ is determined to be 3.26 eV as obtained by Tauc plots (Fig. 6b). The valence-band (VB) position of 6Cu-TiO₂ is determined to be 2.66 eV from XPS spectra (Fig. 6c). The Tauc plots and XPS valence-band spectra of TiO₂ sample are shown in Figs. S4, S5. Accordingly, the energy band diagram and the photocatalytic mechanism can be drawn, as shown in Fig. 6d. During the reaction process, semiconductor material (support) is stimulated by light to produce photogenerated carriers, and the electrons transfer from the conduction band (CB) of TiO₂ to the ultra-fine Cu clusters, resulting in the separation of the photogenerated electrons and holes and thus reducing H₂O to H₂. Notably, ultra-fine Cu clusters as co-catalyst on the surface of TiO₂ will perform as active sites to capture the

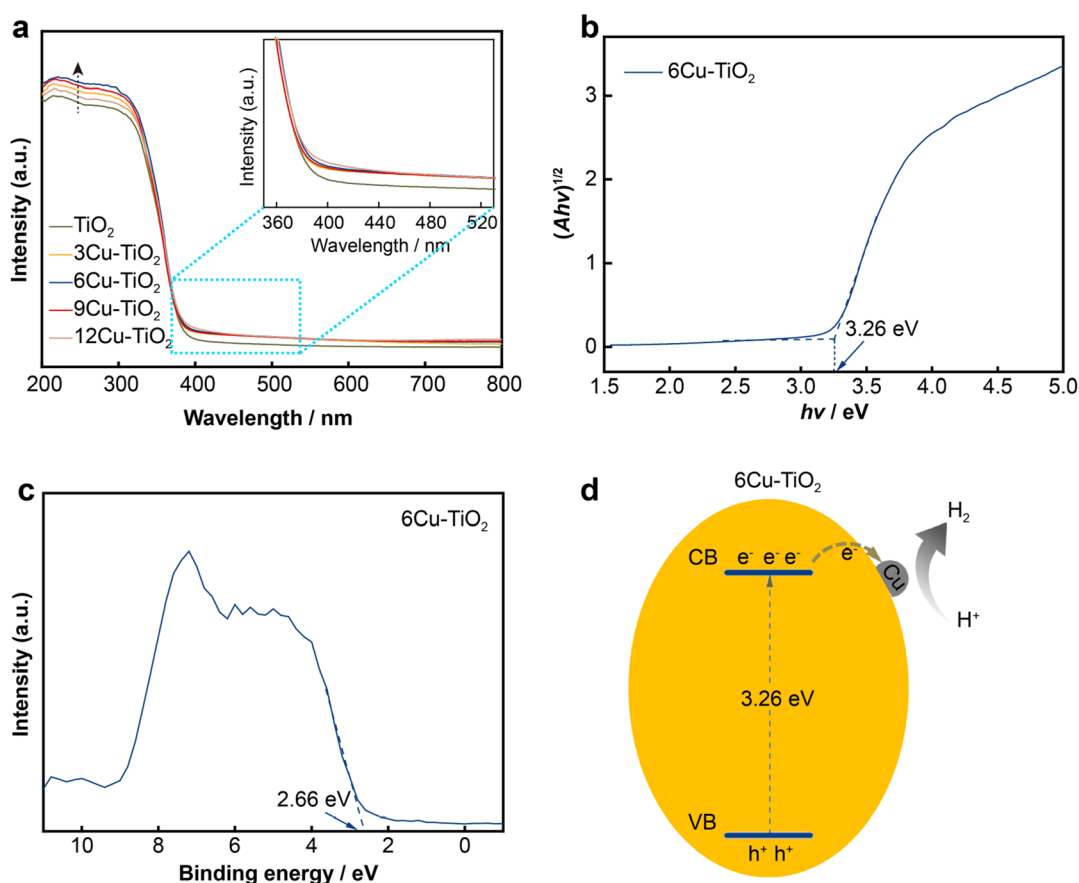


Fig. 6 **a** UV–Vis absorption spectra of samples (enlarged view as inset); **b** Tauc plots and **c** XPS valence-band spectra of 6Cu–TiO₂; **d** energy band diagram of 6Cu–TiO₂

electrons through modulating interfacial charge transfer process and lead to excellent photocatalytic hydrogen evolution performance.

5 Conclusion

In summary, a promising hydrangea-like TiO₂ support with enhanced photocatalytic performance was obtained by a simple hydrothermal method. The hydrangea-like TiO₂ (1.8 mmol·h⁻¹·g⁻¹) shows ~ 10.7 times higher photocatalytic H₂ evolution efficiency than P25 (168 μmol·h⁻¹·g⁻¹). The photocatalytic hydrogen evolution is further improved after ultra-fine (~ 1 nm) Cu clusters loaded onto the surface of the TiO₂. The optimized system 6Cu–TiO₂ (6 wt%) shows a maximal value of 3.7 mmol·h⁻¹·g⁻¹ for hydrogen production, which is approximately twofold higher than that of the bare hydrangea-like TiO₂. The enhanced H₂ production is attributed to the surface electronic structure/properties tuned by the ultra-fine Cu clusters. Both experimental and theoretical results reveal that the charge separation and transfer have been improved after

Cu clusters decoration. In the Cu–TiO₂ systems, the photogenerated electrons tend to transfer from CB of TiO₂ to Cu clusters, which could effectively promote the separation and transfer of photogenerated carriers. Subsequently, the electrons accumulate on the Cu clusters and accelerate the reduction of H₂O to H₂, resulting in high efficiency of photocatalytic hydrogen evolution. More importantly, this work offers a novel route to design high-performance TiO₂ support for high-efficiency photocatalysis.

Acknowledgements This work was financially supported by the National Natural Science Foundation of China (Nos. 11874356, 11904039, 51772035 and 52071041), the Project for Fundamental and Frontier Research in Chongqing (Nos. cstc2019jcyj-jqX0002 and cstc2020jcyj-msxmX0777) and the Fundamental Research Funds for the Central Universities (No. 106112016CDJZR308808). The work conducted at Chongqing Institute of Green and Intelligent Technology (Chinese Academy of Sciences) is also supported by Key Research Program of Frontier Sciences, CAS (No. QYZDB-SSW-SLH016).

Declarations

Conflict of interests The authors declare that they have no conflict of interests.

References

- [1] Green MA, Bremner SP. Energy conversion approaches and materials for high-efficiency photovoltaics. *Nat Mater.* 2016; 16(1):23.
- [2] Tachibana Y, Vayssieres L, Durrant JR. Artificial photosynthesis for solar water-splitting. *Nat Photonics.* 2012;6(8):511.
- [3] Zhu JX, Cheng G, Xiong JY, Li WJ, Dou SX. Recent advances in Cu-based cocatalysts toward solar-to-hydrogen evolution: categories and roles. *Sol RRL.* 2019;3(10):1900256.
- [4] Lei Y, Wang Y, Liu Y, Song C, Li Q, Wang D, Li Y. Realizing the atomic active center for hydrogen evolution electrocatalysts. *Angew Chem Int Ed.* 2020;59(47):20794.
- [5] Wang Q, Domen K. Particulate photocatalysts for light-driven water splitting: mechanisms, challenges, and design strategies. *Chem Rev.* 2019;120(2):919.
- [6] Takata T, Jiang J, Sakata Y, Nakabayashi M, Shibata N, Nandal V, Seki K, Hisatomi T, Domen K. Photocatalytic water splitting with a quantum efficiency of almost unity. *Nature.* 2020; 581(7809):411.
- [7] Fujishima A, Honda K. Electrochemical photolysis of water at a semiconductor electrode. *Nature.* 1972;238(5358):37.
- [8] Zuo GC, Wang YT, Teo WL, Xian QM, Zhao YL. Direct Z-scheme TiO₂-ZnIn₂S₄ nanoflowers for cocatalyst-free photocatalytic watersplitting. *Appl Catal B: Environ.* 2021;291: 120126.
- [9] Sun J, Zhang M, Wang ZF, Chen HY, Chen Y, Murakami N, Ohno T. Synthesis of anatase TiO₂ with exposed {001} and {101} facets and photocatalytic activity. *Rare Met.* 2019;38(4):287.
- [10] Yang DX, Qu D, Miao X, Jiang WS, An L, Wen YJ, Wu DD, Sun ZC. TiO₂ sensitized by red-, green-, blue-emissive carbon dots for enhanced H₂ production. *Rare Met.* 2019; 38(5):404.
- [11] Zuo G, Wang Y, Teo WL, Xian Q, Zhao Y. Direct Z-scheme TiO₂-ZnIn₂S₄ nanoflowers for cocatalyst-free photocatalytic water splitting. *Appl Catal B: Environ.* 2021; 291: 120126.
- [12] Wang C, Wang KW, Feng YB, Li C, Zhou XY, Gan LY, Feng YJ, Zhou HJ, Zhang B, Qu XL, Li H, Li JY, Li A, Sun YY, Zhang SB, Yang G, Guo YZ, Yang SZ, Zhou TH, Dong F, Zheng K, Wang LH, Huang J, Zhang Z, Han XD. Co and Pt dual-single-atoms with oxygen-coordinated Co-O-Pt dimer sites for ultrahigh photocatalytic hydrogen evolution efficiency. *Adv Mater.* 2021;33(13):e2003327.
- [13] Sadanandam G, Luo X, Chen XX, Bao YW, Homewood KP, Gao Y. Cu oxide quantum dots loaded TiO₂ nanosheet photocatalyst for highly efficient and robust hydrogen generation. *Appl Surf Sci.* 2021; 541:148687.
- [14] Li Y, Min KA, Han B, Lee LYS. Ni nanoparticles on active (001) facet-exposed rutile TiO₂ nanopyramid arrays for efficient hydrogen evolution. *Appl Catal B: Environ.* 2021; 282:119548.
- [15] Esmat M, El-Hosainy H, Tahawy R, Jevasuwan W, Tsunoji N, Fukata N, Ide Y. Nitrogen doping-mediated oxygen vacancies enhancing co-catalyst-free solar photocatalytic H₂ production activity in anatase TiO₂ nanosheet assembly. *Appl Catal B: Environ.* 2021; 285:119755.
- [16] Hu X, Song J, Luo J, Zhang H, Sun Z, Li C, Zheng S, Liu Q. Single-atomic Pt sites anchored on defective TiO₂ nanosheets as a superior photocatalyst for hydrogen evolution. *J Energy Chem.* 2021;62:1.
- [17] Guo Q, Zhou C, Ma Z, Yang X. Fundamentals of TiO₂ photocatalysis: concepts, mechanisms, and challenges. *Adv Mater.* 2019;31(50):1901997.
- [18] Kurnaravel V, Mathew S, Bartlett J, Pillai SC. Photocatalytic hydrogen production using metal doped TiO₂: a review of recent advances. *Appl Catal B-Environ.* 2019;244:1021.
- [19] Tabunag JS, Guo YJ, Yu HZ. Interactions between hemin-binding DNA aptamers and hemin-graphene nanosheets: reduced affinity but unperturbed catalytic activity. *J Anal Test.* 2019;3:107.
- [20] Meng A, Zhang L, Cheng B, Yu J. Dual cocatalysts in TiO₂ photocatalysis. *Adv Mater.* 2019;31(30):1807660.
- [21] Zuo Q, Liu T, Chen C, Ji Y, Gong X, Mai Y, Zhou Y. Ultrathin metal-organic framework nanosheets with ultrahigh loading of single Pt atoms for efficient visible-light-driven photocatalytic H₂ evolution. *Angew Chem Int Edit.* 2019;58(30):10198.
- [22] Zhou P, Lv F, Li N, Zhang Y, Mu Z, Tang Y, Lai J, Chao Y, Luo M, Lin F, Zhou J, Su D, Guo S. Strengthening reactive metal-support interaction to stabilize high-density Pt single atoms on electron-deficient g-C₃N₄ for boosting photocatalytic H₂ production. *Nano Energy.* 2019;56:127.
- [23] Hejazi S, Mohajernia S, Osuagwu B, Zoppellaro G, Andryskova P, Tomanec O, Kment S, Zbořil R, Schmuki P. On the controlled loading of single platinum atoms as a co-catalyst on TiO₂ anatase for optimized photocatalytic H₂ generation. *Adv Mater.* 2020;32(16):1908505.
- [24] Fang X, Shang Q, Wang Y, Jiao L, Yao T, Li Y, Zhang Q, Luo Y, Jiang HL. Single Pt atoms confined into a metal-organic framework for efficient photocatalysis. *Adv Mater.* 2018;30(7): 1705112.
- [25] Li X, Bi W, Zhang L, Tao S, Chu W, Zhang Q, Luo Y, Wu C, Xie Y. Single-atom Pt as co-catalyst for enhanced photocatalytic H₂ evolution. *Adv Mater.* 2016;28(12):2427.
- [26] Sui Y, Liu S, Li T, Liu Q, Jiang T, Guo Y, Luo JL. Atomically dispersed Pt on specific TiO₂ facets for photocatalytic H₂ evolution. *J Catal.* 2017;353:250.
- [27] Liu L, Corma A. Metal catalysts for heterogeneous catalysis: from single atoms to nanoclusters and nanoparticles. *Chem Rev.* 2018;118(10):4981.
- [28] Xing J, Chen JF, Li YH, Yuan WT, Zhou Y, Zheng LR, Wang HF, Hu P, Wang Y, Zhao HJ, Wang Y, Yang HG. Stable isolated metal atoms as active sites for photocatalytic hydrogen evolution. *Chem Eur J.* 2014;20(8):2138.
- [29] Yi L, Lan F, Li J, Zhao C. Efficient noble-metal-free Co-NG/TiO₂ photocatalyst for H₂ evolution: synergistic effect between single-atom Co and N-doped graphene for enhanced photocatalytic activity. *ACS Sustain Chem Eng.* 2018;6(10):12766.
- [30] Walmsley JD, Hill JW, Saha P, Hill CM. Probing electrocatalytic CO₂ reduction at individual Cu nanostructures via optically targeted electrochemical cell microscopy. *J Anal Test.* 2019;3:140.
- [31] Liu W, Cao L, Cheng W, Cao Y, Liu X, Zhang W, Mou X, Jin L, Zheng X, Che W, Liu Q, Yao T, Wei S. Single-site active cobalt-based photocatalyst with a long carrier lifetime for spontaneous overall water splitting. *Angew Chem Int Edit.* 2017;56(32):9312.
- [32] Jo WK, Jin YJ. 2D graphene-assisted low-cost metal (Ag, Cu, Fe, or Ni)-doped TiO₂ nanowire architectures for enhanced hydrogen generation. *J Alloy and Comp.* 2018;765:106.
- [33] Xiao M, Zhang L, Luo B, Lyu M, Wang Z, Huang H, Wang S, Du A, Wang L. Molten-salt-mediated synthesis of an atomic nickel co-catalyst on TiO₂ for improved photocatalytic H₂ evolution. *Angew Chem Int Edit.* 2020;132(18):7297.
- [34] Jin X, Wang R, Zhang L, Si R, Shen M, Wang M, Tian J, Shi J. Electron configuration modulation of nickel single atoms for elevated photocatalytic hydrogen evolution. *Angew Chem Int Edit.* 2020;132(17):6894.
- [35] Naldoni A, Altomare M, Zoppellaro G, Liu N, Kment S, Zboril R, Schmuki P. Photocatalysis with reduced TiO₂: from black TiO₂ to cocatalyst-free hydrogen production. *ACS Catal.* 2019; 9(1):345.

- [36] Wan J, Chen W, Jia C, Zheng L, Dong J, Zheng X, Wang Y, Yan W, Chen C, Peng Q, Wang D, Li Y. Defect effects on TiO₂ nanosheets: stabilizing single atomic site Au and promoting catalytic properties. *Adv Mater.* 2018;30(11):1705369.
- [37] Gao M, Zhu L, Ong WL, Wang J, Ho GW. Structural design of TiO₂-based photocatalyst for H₂ production and degradation applications. *Catal Sci Technol.* 2015;5(10):4703.
- [38] Ye J, Liu W, Cai J, Chen S, Zhao X, Zhou H, Qi L. Nanoporous anatase TiO₂ mesocrystals: additive-free synthesis, remarkable crystalline-phase stability, and improved lithium insertion behavior. *J Am Chem Soc.* 2011;133(4):933.
- [39] Zhu T, Li J, Wu Q. Construction of TiO₂ hierarchical nanostructures from nanocrystals and their photocatalytic properties. *ACS Appl Mater Inter.* 2011;3(9):3448.
- [40] Chen Y, Li S, Zhao RY, Li W, Ren ZH, Han GR. Single-crystal TiO₂/SrTiO₃ core-shell heterostructured nanowire arrays for enhanced photoelectrochemical performance. *Rare Met.* 2019;38(5):369.
- [41] Yuan L, Han C, Yang MQ, Xu YJ. Photocatalytic water splitting for solar hydrogen generation: fundamentals and recent advancements. *Int Rev in Phys Chem.* 2016;35(1):1.
- [42] Li R, Li C. Photocatalytic water splitting on semiconductor-based photocatalysts. *Adv Catal.* 2017;60:1.
- [43] Zhu S, Chen XF, Li ZC, Ye XY, Liu Y, Chen Y, Yang L, Chen M, Zhang DQ, Li GS, Li HX. Cooperation between inside and outside of TiO₂: lattice Cu⁺ accelerates carrier migration to the surface of metal copper for photocatalytic CO₂ reduction. *Appl Catal B: Environ.* 2020; 264:118515.
- [44] Peng M, Dong CY, Gao R, Xiao DQ, Liu H, Ma D. Fully exposed cluster catalyst (FECC): toward rich surface sites and full atom utilization efficiency. *ACS Central Sci.* 2021;7(2):262.
- [45] Wang T, Tao X, Li X, Zhang K, Liu S, Li B. Synergistic Pd single atoms, clusters, and oxygen vacancies on TiO₂ for photocatalytic hydrogen evolution coupled with selective organic oxidation. *Small.* 2020;17(2):2006255.
- [46] Zhang H, Zhang P, Qiu M, Dong J, Zhang Y, Lou XWD. Ultrasmall MoO_x clusters as a novel cocatalyst for photocatalytic hydrogen evolution. *Adv Mater.* 2019;31(6):1804883.
- [47] Yan QQ, Wu DX, Chu SQ, Chen ZQ, Lin Y, Chen MX, Zhang J, Wu XJ, Liang HW. Reversing the charge transfer between platinum and sulfur-doped carbon support for electrocatalytic hydrogen evolution. *Nat Commun.* 2019;10(1):1.
- [48] Ji S, Chen Y, Fu Q, Chen Y, Dong J, Chen W, Li Z, Wang Y, Gu L, He W, Chen C, Peng Q, Huang Y, Duan X, Wang D, Draxl C, Li Y. Confined pyrolysis within metal-organic frameworks to form uniform Ru₃ clusters for efficient oxidation of alcohols. *J Am Chem Soc.* 2017;139(29):9795.
- [49] Lee BH, Park S, Kim M, Sinha AK, Lee SC, Jung E, Chang WJ, Lee KS, Kim JH, Cho SP, Kim H, Nam KT, Hyeon T. Reversible and cooperative photoactivation of single-atom Cu/TiO₂ photocatalysts. *Nat Mater.* 2019;18(6):620.
- [50] Seadira TWP, Sadanandam G, Ntho T, Masuku CM, Scurrill MS. Preparation and characterization of metals supported on nanostructured TiO₂ hollow spheres for production of hydrogen via photocatalytic reforming of glycerol. *Appl Catal B: Environ.* 2018;222:133.
- [51] Kresse G, Furthmüller J. Efficient iterative schemes for ab initio total-energy calculations using a plane-wave basis set. *Phys Rev B.* 1996;54(16):11169.
- [52] Kresse G, Furthmüller J. Efficiency of ab-initio total energy calculations for metals and semiconductors using a plane-wave basis set. *Comp Mater Sci.* 1996;6(1):15.
- [53] Filippi C, Singh DJ, Umrigar CJ. All-electron local-density and generalized-gradient calculations of the structural properties of semiconductors. *Phys Rev B.* 1994;50(20):14947.
- [54] Perdew JP, Burke K, Ernzerhof M. Generalized gradient approximation made simple. *Phys Rev Lett.* 1996;77(18):3865.
- [55] Grimme S, Antony J, Ehrlich S, Krieg H. A consistent and accurate ab initio parametrization of density functional dispersion correction (DFT-D) for the 94 elements H-Pu. *J Chem Phys.* 2010;132(15):154104.
- [56] Li J, Zhang M, Guan Z, Li Q, He C, Yang J. Synergistic effect of surface and bulk single-electron-trapped oxygen vacancy of TiO₂ in the photocatalytic reduction of CO₂. *Appl Catal B: Environ.* 2017;206:300.
- [57] Wu T, Zhao H, Zhu X, Xing Z, Liu Q, Liu T, Gao S, Lu S, Chen G, Asiri AM, Zhang Y, Sun X. Identifying the origin of Ti³⁺ activity toward enhanced electrocatalytic N₂ reduction over TiO₂ nanoparticles modulated by mixed-valent copper. *Adv Mater.* 2020;32(30):2000299.
- [58] Zhang H, Cai J, Wang Y, Wu M, Meng M, Tian Y, Li X, Zhang J, Zheng L, Jiang Z, Gong J. Insights into the effects of surface/bulk defects on photocatalytic hydrogen evolution over TiO₂ with exposed {001} facets. *Appl Catal B: Environ.* 2018;220:126.
- [59] Wang Z, Mao X, Chen P, Xiao M, Monny SA, Wang S, Konarova M, Du A, Wang L. Understanding the roles of oxygen vacancies in hematite-based photoelectrochemical processes. *Angew Chem Int Edit.* 2019;58(4):1030.
- [60] Qu D, Liu J, Miao X, Han M, Zhang H, Cui Z, Sun S, Kang Z, Fan H, Sun Z. Peering into water splitting mechanism of g-C₃N₄-carbon dots metal-free photocatalyst. *Appl Catal B: Environ.* 2018;227:418.